Magazine of Concrete Research
Volume 66 Issue 6

Influence of the relative rib area on bond behaviour
Metelli and Plizzari

Magazine of Concrete Research, 2014, **66**(6), 277–294
http://dx.doi.org/10.1680/macr.13.00198
Paper 1300198
Received 09/07/2013; revised 26/11/2013; accepted 27/11/2013
Published online ahead of print 24/01/2014

ice
Institution of Civil Engineers
publishing

Influence of the relative rib area on bond behaviour

Giovanni Metelli
Assistant Professor, Department DICATAM, University of Brescia, Brescia, Italy

Giovanni A. Plizzari
Professor, Department DICATAM, University of Brescia, Brescia, Italy

Steel-to-concrete bond is a basic aspect of the behaviour of reinforced concrete structures both at serviceability and ultimate states. When bond rules were originally developed, experimental results were mainly obtained on normal-strength concrete and a minimum relative rib area (bond index) was required by building codes to ensure good bond properties. The arrival into the market of high-performance concrete and newer structural needs may require different bond indexes. In the present paper, the experimental results of pull-out tests on short anchorages are presented. Several pull-out tests on ribbed bars, embedded in cubes of normal- and high-strength concrete with a concrete cover of 4·5 times the bar diameter, were carried out in order to better understand the influence of the relative rib area and bar diameter on the local bond behaviour, as well as on the splitting crack width generated by the wedging action of ribs. A total of 96 tests were performed on machined bars of three different diameters (12, 16 and 20 mm) with a bond index ranging from 0·040 to 0·105. The results of 55 pull-out tests on commercial hot-rolled ribbed bars of four different diameters (12, 20, 40 and 50 mm) are also presented to confirm that the bond response also depends on bar diameter (size effect). Experimental results provide information concerning the influence of the relative rib area on bond strength and on the bursting force due to the rib's wedge action. As the minimum measured bond strength of rebars was always markedly greater than the minimum bond strength required by building codes even when low bond indexes were adopted, the test results point out the possibility of reducing the minimum value of the relative rib area required by Eurocode 2 without limiting the safety coefficient of bond. The reduction also allows a higher structural ductility that can be achieved due to a greater strain penetration of the rebars from concrete cracks.

Notation

A	nominal cross-sectional area of bar
A_{gt}	elongation at maximum tensile force
a	rib height
b	rib width
c	concrete cover
d	nominal diameter of reinforcing bar
d_e	external diameter of reinforcing bar
d_i	core diameter of reinforcing bar
E_{cm}	mean value of the modulus of elasticity of concrete
f_{bd}	design bond strength
$f_{bd,0}$	basic bond strength
f_{cm}	mean value of concrete compressive strength (cylinder)
$f_{cm,cube}$	mean value of concrete compressive strength (cube)
f_{ctm}	mean value of concrete tensile strength
f_R	measured bond index (or relative rib area)
f_{Rm}	measured mean bond index in each series
$f_{s,0·2}$	tensile strength at 0·2% of the residual deformation
f_{um}	mean ultimate strength of steel
f_{yk}	characteristic yield strength of steel
f_{ym}	mean yield strength of steel
L	bonded length
P	load
s	rib spacing
w	transverse deformation
w_{15}	transverse deformation at a bond stress of 15 MPa
α	rib face inclination
α_2	factor taking into account the confining effects of concrete
β	rib inclination
γ_{cb}	partial safety coefficient for bond
δ_l	loaded-end slip
δ_u	unloaded-end slip
δ_1	slip of 1 mm
τ	bond stress
τ_{bmax}	maximum bond stress for a pull-out failure in Model Code 2010 (fib, 2014)
τ_{max}	bond strength
$\tau_{max,av}$	average bond strength for each series
τ'_{max}	normalised bond strength
$\tau'_{max,av}$	average normalised bond strength for each series
$\tau_{u,split}$	bond strength for splitting failure
$\tau_{0·1}$	bond stress at 0·1 mm unloaded-end slip

Introduction

Steel-to-concrete bond allows longitudinal forces to be transferred from the reinforcement to the surrounding concrete in a reinforced concrete (RC) structure. Due to this stress transfer, the force in a reinforcing bar changes along its length, as does the stress in the concrete embedment. Wherever steel strains differ from concrete strains, a relative displacement between the steel and the concrete occurs (slip). Bond is commonly defined as the rate of change in force along the bar divided by the (nominal) area of bar surface over which that change takes place. However, this simple concept is quite inaccurate since the majority of bars employed today rely on the bearing of the ribs that are made to increase the bond resistance.

Due to the bursting forces on the surrounding concrete as a result of the wedge action of the ribs (Cairns and Jones, 1995a, 1995b), it has been observed that splitting cracks may develop longitudinally along the bar (Gambarova and Rosati, 1997; Giuriani *et al.*, 1991; Tepfers, 1973). Splitting cracks impair bond mechanical behaviour and make the bond very sensitive to confinement (Plizzari *et al.*, 1998; Tepfers, 1973). After splitting, the confining action along the anchored bars or splices is produced by transverse reinforcement (Eligehausen *et al.*, 1983), by external transverse pressure and by cohesive stresses between the splitting crack faces (Darwin *et al.*, 1992; Reinhardt and van der Veen, 1990; Walker *et al.*, 1999; Xu *et al.*, 2011). The latter confining action underlines the potential benefit of fibre reinforcement in concrete (Harajli *et al.*, 1995; Jansson *et al.*, 2012), even though recent studies have shown that the addition of fibres can cause a reduction in bond strength due to disturbance in the concrete matrix near the bar ribs (Dancygier and Katz, 2010).

When splitting of concrete occurs, another important aspect is structural durability. Most building codes do not have requirements on splitting crack width, whose limits should be more severe than for flexural cracks. In fact, while the latter exposes a very limited bar length to the environment, splitting cracks develop longitudinally along the bar so that a considerable length of the reinforcement can be exposed to aggressive agents (Giuriani and Plizzari, 1998).

Detailed evaluation of bond strength and bond performance is complex, as the magnitude of bond strength is influenced by a wide range of factors. As an example, Model Code 2010 (MC2010) includes about ten parameters for determining anchorage or splice strength (fib, 2013). A survey of published literature on bonding was presented by Gambarova *et al.* (2000).

Depending on cover and confinement, different modes of bond failure are possible – pull-out failure and splitting failure. In the former case, bond failure is mostly due to the shearing off of the concrete keys cast between each pair of lugs (Cairns and Abdullah, 1995; Giuriani, 1982). In the latter case, bond failure is mostly due to the longitudinal splitting of the concrete surrounding the bar (Cairns and Jones, 1995a).

The bond between reinforcement and concrete governs several mechanisms in RC structures, such as those related to anchorage and splice, shear behaviour and cracking. Steel-to-concrete bond should fulfil the following requirements.

(*a*) At service conditions, small flexural and splitting crack width and limited deflection of RC members should be ensured.
(*b*) At ultimate state, anchorages and lapped splice strength should be guaranteed.
(*c*) After yielding of the rebars, large rotation capacity at plastic hinges should be required to provide adequate ductility and energy dissipation to the structural element (Eligehausen and Mayer, 2000; Wildermuth and Hofmann, 2012).

Since these requirements are partly contradictory for bond properties, a compromise may represent an optimised solution for the rib geometry.

A review of previous studies (Cairns and Jones, 1995b; Darwin and Graham, 1993; Eligehausen and Mayer, 2000; Rhem, 1969) shows that the main rib parameter influencing bond strength and stiffness is the relative rib area, or bond index (f_R), which is defined as the ratio between the rib area above the core, projected on a plane perpendicular to the bar axis, and the nominal bar surface area between two contiguous ribs.

When bond rules were originally developed, experimental results available in the literature were mainly obtained on normal-size rebars in normal-strength concrete (NSC). Based on these results, a minimum bond index was required by building codes to ensure good bond properties (Cairns and Plizzari, 2003). As an example, according to Eurocode 2 (CEN, 2004), a minimum bond index of 0·056 is required for a diameter larger than 12 mm in order to guarantee the required bond stiffness and strength.

As far as the influence of the bond index is concerned, by performing beam-end tests, Darwin and Graham (1993) showed a small increase in bond strength (10%) when the bond index varied from 0·05 to 0·2 in bars well confined by concrete cover and transverse reinforcement; the bond–slip response was also independent of the combination of rib height and spacing. Experimental and theoretical studies on the strength of lapped joints carried out by Cairns and Jones (1995b) showed that, by doubling the bond index (from 0·05 to 0·10), the bond strength increased by 30% because of the lower bursting force generated by more highly ribbed bars.

Zuo and Darwin (2000) studied the effect of the bond index on bond–slip behaviour when reversed cyclic loading was applied; the test results showed a significant reduction of the unloaded-end slip (up to 70%) when the bond index increased from 0·085 to 0·119. As a result, the use of high relative rib area bars may reduce the bond damage but, at the same time, might favour strain localisation, thus limiting the rotation capacity of plastic hinges in RC structures (Eligehausen and Mayer, 2000;

Wildermuth and Hofmann, 2012). Numerical simulations carried out by Wildermuth and Hofmann (2012) showed an increase in the plastic rotation of a beam by more than 50% when the bond index decreased from 0·09 to 0·02 and by 20% when the bond index decreased from 0·09 to 0·07.

There is therefore a need to optimise the relative rib area in order to obtain a good bond strength for anchorages as well as an enhanced plastic hinge (possible with lower bond strength and stiffness) for structural ductility. Furthermore, the arrival into the market of high-performance concrete and newer structural needs may require different bond indexes.

The aim of the present research work was to investigate the influence of rib geometry on the bond strength and stiffness, as well as on the splitting cracks due to the bursting forces generated by the wedge action of the ribs. Several pull-out tests were performed on rebars with different diameters and rib geometries. Furthermore, the size effect on bond behaviour was also studied by performing pull-out tests on large rebars of diameter 40 mm and 50 mm.

Experimental work and materials

Twelve series of pull-out tests were performed on concrete specimens (cubes) with an embedded bar having a nominal diameter (d) of 12, 16 or 20 mm. The bar diameters were chosen in order to obtain an approximately constant ratio between the bonded surfaces of two contiguous diameters ($A_{20}/A_{16} = 1{\cdot}56$; $A_{16}/A_{12} = 1{\cdot}78$).

For each bar diameter, two values of the bond index (f_R) were investigated – a lower bond index value, close to 0·065, and an upper value, close to 0·095, for 16 mm and 20 mm diameter bars; the 12 mm bars (with a lower minimum requirement by codes) had a bond index ranging between 0·040 (lower) and 0·096 (upper).

Smooth bars were machined in order to obtain helical ribs adopting a commonly used trapezoidal profile with an inclination (β) of roughly 80° to the bar axis and a rib face inclination (α) of 50° (Figure 1). The rib spacing (s) varied between 6·0 mm and 13·9 mm in the 12 mm and 20 mm bars respectively. The conventional value of the ratio between the nominal diameter (d) and the rib height (a) was constant and equal to 22, with the exception of the 12 mm bars (with $f_{Rm} = 0{\cdot}047$), where the ratio was 32. The measurement of rib height (a) and external bar diameter (d_e) were taken at 120° intervals along the helical ribs and averaged. For each bar, the bond index was calculated using

$$1. \quad f_R = \frac{d_e^2 - d_i^2}{4ds}$$

$$2. \quad d_i = d_e - 2a$$

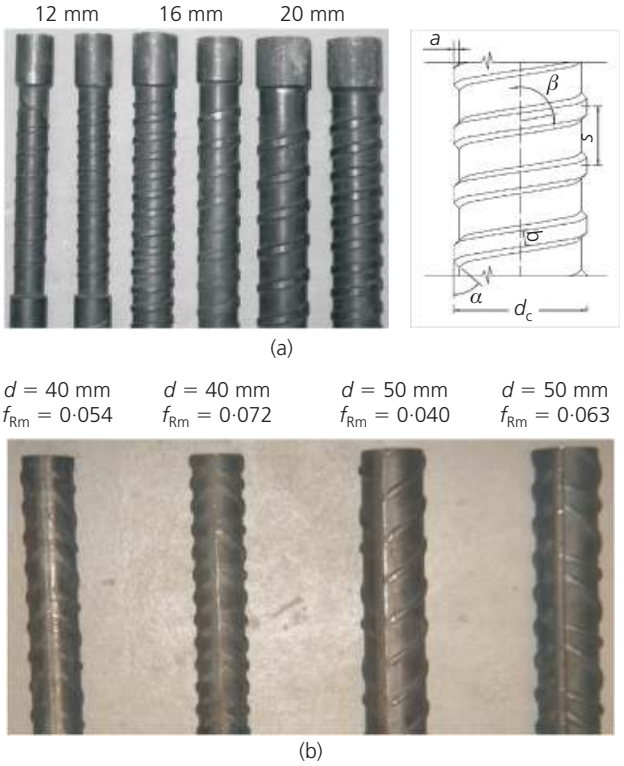

Figure 1. (a) Machined ribbed bars and geometry. (b) Hot-rolled commercial bars

in which d_e is the external bar diameter (top of the rib), d_i is the core diameter (bottom of the rib), d is the nominal diameter, s is longitudinal spacing of the ribs and a is the rib height. The geometric properties of the machined steel bars are shown in Figure 1(a) and listed in Table 1 (also see the Appendix).

High-grade steel was used with a mean yield strength (f_{ym}) of 940 MPa in order to prevent the bar yielding before bond failure (Table 2). As each series consisted of eight specimens and the bars were tested both in normal- and high-strength concrete (NSC and HSC), 96 specimens with an embedded machined bar were tested.

A further eight series of pull-out tests, consisting of five specimens each (at least), were performed on commercial hot-rolled bars of diameter 12, 20, 40 and 50 mm. The 12 and 20 mm ribbed bars were characterised by a bond index greater than the minimum required by Eurocode 2 and they were tested both in NSC and HSC; the 40 and 50 mm diameter bars were tested only in NSC. For each large-diameter bar, two values of the bond index were investigated (Figure 1(b))

- lower than the minimum value required by Eurocode 2 ($f_{Rm} = 0{\cdot}040$ or $f_{Rm} = 0{\cdot}054$ respectively for 50 and 40 mm bar diameters)
- greater than the minimum value required by Eurocode 2

Magazine of Concrete Research 2014.66:277-294.

d: mm	f_{Rm}	d_e: mm	β: degrees	s: mm	a: mm	b: mm	α: degrees
12	0·047	13	77·90	8·50	0·38	1·5	50
12	0·081	13	81·65	6·00	0·55	1·5	50
16	0·061	17	78·40	10·95	0·70	2·0	50
16	0·095	17	82·00	7·50	0·70	2·0	50
20	0·065	21	78·10	13·90	0·90	2·5	50
20	0·092	21	81·80	9·50	0·90	2·5	50

Table 1. Geometric properties of the machined reinforcing bars (nominal values)

	d: mm	f_R	f_{ym}: MPa	f_{um}: MPa	A_{gt}: %
Machined bars					
	12–20	0·040–0·105	940	1040	3·5
Hot-rolled commercial bars – grade 500					
	20	0·079–0·089	540	680	13·1
	40	0·054	542	677	13·3
	40	0·072	524	663	14·3
	50	0·040	560	752	14·4
	50	0·063	552	724	13·6
Hot-rolled commercial bars – grade 700					
	12	0·095–0·105	650	742[a]	—

[a] Note this value is for $f_{s,0·2}$ (in MPa).

Table 2. Mechanical properties of the reinforcing bars

($f_{Rm} = 0·063$ or $f_{Rm} = 0·072$ respectively for 50 and 40 mm bar diameters).

The large bars were tested only in NSC. The relative rib area of each hot-rolled bar was measured according to ISO 15630-1 (ISO, 2010). A normal steel was used for 20, 40 and 50 mm diameter bars, with a mean yield strength $f_{ym} = 524–560$ MPa (Table 2). The 12 mm diameter bars were made of steel with a higher strength ($f_{ym} = 704$ MPa).

The concrete was poured into wooden forms with the bars in a horizontal position in order to obtain homogeneous bond conditions along the anchorage length. Specimens were cast in groups of nine (three series, each consisting of three specimens) from a single batch of concrete. The concrete mix proportions are shown in Table 3; the aggregates for the mix were defined by weight according to the percentages shown in Table 4.

The cast specimens were left for 36 h and then demoulded and stored in a humidity room at constant 90% humidity and temperature 20°C until the time of the test. From each batch, four cylindrical samples (80 mm diameter, 160 mm high) and

d: mm	Concrete	Cement: kg/m^3	Water: l/m^3	w/c	Aggregate: kg/m^3	Superplasticiser: l/m^3
40, 50	NSC	325 (R325)	160	0·49	1949	3·0
12, 16, 20	NSC	350 (R425)	180	0·51	1815	3·5
12, 16, 20	HSC	450 (R525)	142	0·32	1885	5·0

Table 3. Composition of normal-strength and high-strength concretes

Grain class: mm	Percentage: %	
	NSC	HSC
0·00–0·35	10·56	7·12
0·35–0·45	12·72	9·36
0·40–0·60	15·55	12·30
0·60–1·50	27·82	25·04
1·50–2·50	37·53	35·13
2·50–3·50	48·95	46·98
4·00–6·00	61·20	59·71
7·00–12·00	80·63	79·88
10·00–15·00	100·00	100·00

Table 4. Aggregate composition in normal-strength and high-strength concretes

eight cubes (side 150 mm) were cast and cured in the same conditions as the pull-out specimens. At the time of testing, the NSC specimens presented a compressive cubic strength $f_{cm,cube} = 42{\cdot}7–47{\cdot}8$ MPa, while the compressive strength of the HSC specimens ranged between 63·4 MPa and 74·3 MPa (average values). The curing time and the mechanical characteristics of the concrete specimens are summarised in Table 5.

For the specimens with a large bar diameter, the concrete was poured into wooden forms with the bars in a horizontal position. The 24 specimens were demoulded 24 h after casting and were then stored in the laboratory at a temperature of about 22°C and relative humidity about 45%. As shown in Table 5, at the time of testing, the concrete compressive strength ($f_{cm,cube}$) of the specimens with large bars was 37·6 MPa.

Test set-up

The test equipment (Figure 2) used was as for a typical pull-out test proposed by Rilem/CEB/FIP (1978). The specimen was characterised by an embedded length of five bar diameters in a concrete cube having a side of ten bar diameters. A plastic sleeve rendered the rebar unbonded over half the depth of the cubic specimen (five bar diameters) and a 2 mm thick Teflon sheet reduced friction at the bearing surface of the specimen.

During the test, the unloaded-end slip (δ_u) was measured by a linear variable differential transformer (LVDT) centrally mounted on the bar while the loaded-end slip (δ_l) was measured by two

Series	d: mm	f_{Rm}	Curing time: days	$f_{cm,cube}$: MPa	f_{ctm}: MPa	E_{cm}: MPa
1	12	0·047	34	42·72	3·4	26 672
2	16	0·061				
3	20	0·065				
4	12	0·081	29	47·82	4·3	28 059
5	16	0·095				
6	20	0·092				
7	12	0·047	28	63·40	4·3	31 024
8	16	0·061				
9	20	0·065				
10	12	0·081	21	74·33	4·5	30 215
11	16	0·095				
12	20	0·092				
13	12	0·095	38	41·50	3·4	29 733
14	20	0·089				
15	12	0·089	90	64·80	3·2	33 270
16	20	0·079				
17	40	0·054	40	37·60	3·0	26 500
18	40	0·072				
19	50	0·040				
20	50	0·063				

f_{Rm} = average value of the actual bond index; $f_{cm,cube}$ = mean compressive strength from eight cubes; f_{ctm} = mean tensile strength from two cylinders; E_{cm} = mean tangent modulus of elasticity from two cylinders.

Table 5. Mechanical properties of the concrete specimens

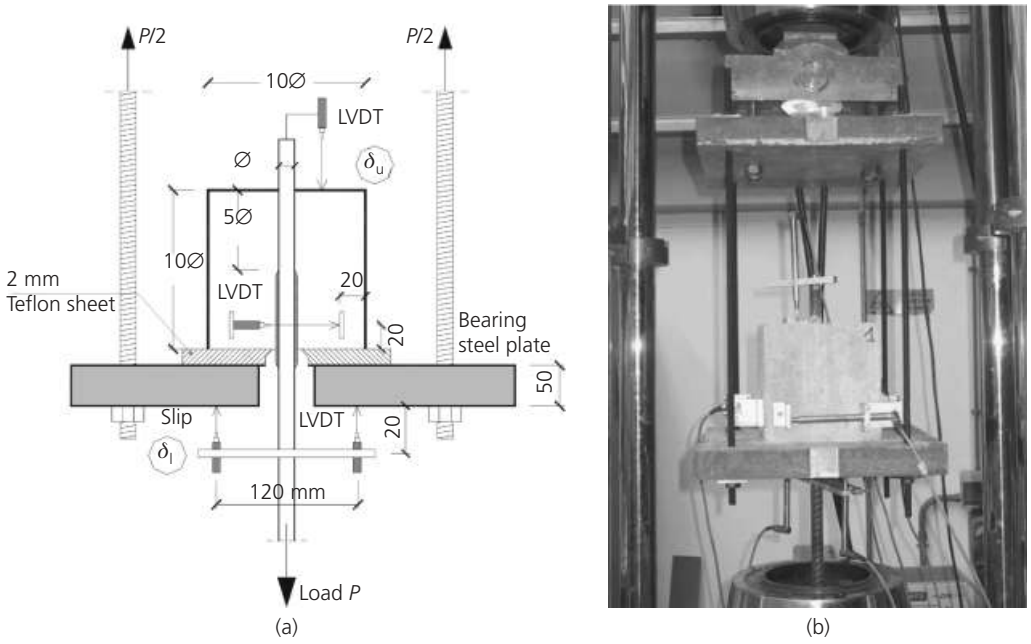

Figure 2. (a) Test set-up for normal-size bars. (b) A specimen and instrumentation

LVDTs placed at 180°, as shown in Figure 2. An LVDT placed on each side face of the specimen, at a distance of 20 mm from the Teflon–concrete interface, provided the transverse deformation w (including the splitting crack, where present). The latter measurement can provide information on the deformation or on the splitting crack due to bursting forces generated by the bond action.

The tests were displacement controlled up to failure with a loaded-end displacement rate of 0·1 mm/min. The displacement rate was calibrated in order to obtain accurate data of the ascending branch of the bond–slip relationship, with a single test lasting about 2 h.

Due to their dimensions, the specimens with large-diameter bars were tested horizontally, with a hydraulic jack to apply the load (Figure 3). The tests were load controlled with a load rate of 0·9 and 1·4 kN/s for the 40 and 50 mm bar diameters respectively. As for the normal-size bars, the unloaded-end slip and the loaded-end slip were measured. Further details can be found in the literature (Metelli *et al.*, 2010).

Test results and discussion

The experimental results concern the bond stress τ, the unloaded-end slip δ_u and the transverse deformation w for the 151 specimens, characterised by five diameters, two concrete grades and a bond index in the range 0·04 to 0·105. Mean values from a single series of hot-rolled commercial bars were generally considered and compared to the results of specimens with the machined bar.

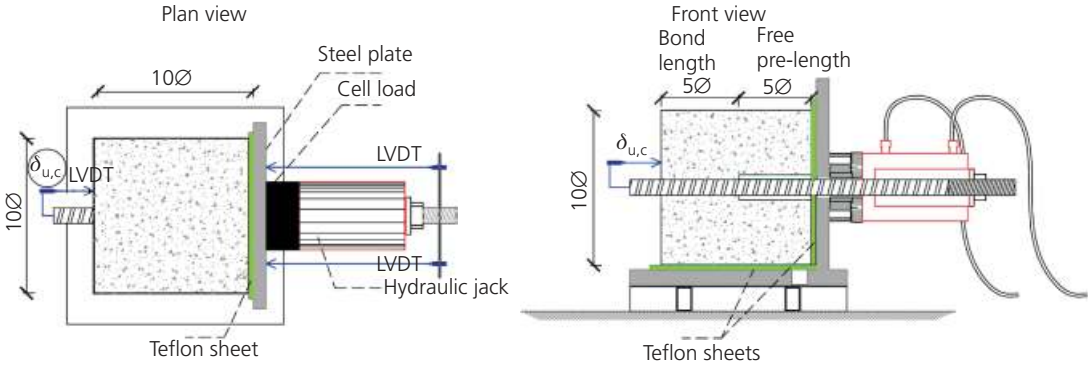

Figure 3. Test set-up for large-diameter bars

With regard to the machined bars, all 48 HSC specimens were tested successfully. Two tests in NSC, concerning a 12 mm and a 20 mm bar, were discarded because the testing machine could not control the tests accurately. Furthermore, five specimens with results having a relative deviation greater than 30% within the same series were neglected.

Since a short anchorage length was used, the bond stress τ is conventionally assumed to be uniformly distributed along the embedded surface of the rebar and it is evaluated by

$$\tau = P/\pi dL \quad (3)$$

where P is the applied load, d is the nominal bar diameter and L is the nominal bonded length (equal to $5d$).

The main experimental results are listed in Table 6 for the machined bars and Table 7 for hot-rolled commercial bars. As far as the machined bars are concerned, most of the specimens failed because of the development of a splitting crack on a longitudinal plane including the bar axis (Figure 4); the only exceptions were found in seven HSC specimens with a rebar having a bond index of about 0·065 (three 16 mm machined bars and four 20 mm machined bars), in one NSC specimen with a 12 mm machined bar (having a bond index of 0·075) and in six specimens with commercial bars that suffered pull-out failure.

Comparison of the bond stress (τ) versus unloaded-end slip (δ_u) curves between series with different bond indexes but the same diameter and concrete strength are shown in Figure 5. Figure 6 shows the same comparison between series with a different concrete strength but the same bond index and bar diameter. Each series, consisting of eight specimens of normal-size diameter (12, 16 and 20 mm) and at least five specimens of large-diameter (40 and 50 mm) bars, is labelled by the average value of the measured bond index f_{Rm}. The curves show better behaviour of the specimens with a greater bond index or concrete strength, both in terms of bond strength and stiffness.

Specimen	f_R	P_{max}: kN	τ_{max}: MPa	$\tau_{0·1}$: MPa	w_{15}: mm	Failure mode	$\tau_{max,av}$: MPa	$\tau_{max,av}/f_{bd}$ (MC2010)
Series 1, $f_{Rm} = 0·047$, $f_{cm} = 42·7$ MPa, $d = 12$ mm								
1	0·043	—	—	11·52	—	—	25·7	7·99
2	0·058	59·7	26·38	13·63	0·013	SPL		
3	0·042	62·6	27·69	15·43	0·011	SPL		
4	0·057	60·5	26·76	16·53	0·015	SPL		
5[a]	0·040	37·5	16·57	15·84	0·024	SPL		
6	0·052	45·3	20·02	16·07	0·010	SPL		
7	0·043	60·5	26·74	12·95	0·020	SPL		
8	0·040	60·6	26·81	13·46	0·012	SPL		
Series 2, $f_{Rm} = 0·061$, $f_{cm} = 42·7$ MPa, $d = 16$ mm								
9	0·058	92·0	22·88	6·00	0·030	SPL	22·9	7·11
10	0·065	108·7	27·04	6·05	0·008	SPL		
11	0·056	86·7	21·56	7·95	0·016	SPL		
12	0·061	99·5	24·75	11·64	0·022	SPL		
13[a]	0·059	61·4	15·28	7·95	0·030	SPL		
14	0·063	79·9	19·86	9·85	0·023	SPL		
15	0·058	78·8	19·58	12·64	0·027	SPL		
16	0·066	98·8	24·57	8·40	0·017	SPL		
Series 3, $f_{Rm} = 0·065$, $f_{cm} = 42·7$ MPa, $d = 20$ mm								
17	0·063	120·1	19·11	—	—	SPL	20·9	6·49
18	0·073	144·8	23·04	5·22	0·020	SPL		
19	0·068	141·9	22·58	5·20	0·021	SPL		
20	0·049	147·3	23·45	6·19	0·027	SPL		
21	0·066	128·1	20·39	8·14	0·023	SPL		
22	0·069	129·0	20·53	6·23	0·031	SPL		
23[a]	0·063	84·7	13·48	13·24	—	SPL		
24	0·069	108·5	17·26	8·14	0·015	SPL		

Table 6. Summary of test results of machined bars (continued on next page)

Specimen	f_R	P_{max}: kN	τ_{max}: MPa	$\tau_{0\cdot1}$: MPa	w_{15}: mm	Failure mode	$\tau_{max,av}$: MPa	$\tau_{max,av}/f_{bd}$ (MC2010)
Series 4, $f_{Rm} = 0{\cdot}081$, $f_{cm} = 47{\cdot}8$ MPa, $d = 12$ mm								
25	0·076	55·8	24·68	13·46	—	SPL	28·9	8·39
26	0·084	65·1	28·78	18·20	0·014	SPL		
27	0·083	68·1	30·09	18·62	0·021	SPL		
28	0·082	66·6	29·45	19·24	0·018	SPL		
29	0·077	60·3	26·65	14·45	0·019	SPL		
30	0·075	63·1	27·92	14·68	0·008	PO		
31	0·096	76·8	33·96	21·44	0·004	SPL		
32	0·079	67·3	29·74	15·06	0·017	SPL		
Series 5, $f_{Rm} = 0{\cdot}095$, $f_{cm} = 47{\cdot}8$ MPa, $d = 16$ mm								
33	0·086	103·9	25·83	9·89	0·013	SPL	25·5	7·41
34	0·095	91·4	22·73	14·35	0·034	SPL		
35	0·097	100·8	25·06	14·70	0·013	SPL		
36	0·096	104·8	26·05	12·94	0·009	SPL		
37	0·105	121·4	30·18	15·64	0·011	SPL		
38	0·094	114·7	28·53	13·03	0·009	SPL		
39	0·097	85·4	21·24	14·65	0·022	SPL		
40	0·093	98·5	24·49	13·06	0·010	SPL		
Series 6, $f_{Rm} = 0{\cdot}092$, $f_{cm} = 47{\cdot}8$ MPa, $d = 20$ mm								
41	0·089	131·1	20·87	12·60	0·011	SPL	25·5	7·41
42	0·100	157·9	25·13	16·98	0·001	SPL		
43	0·086	167·6	26·67	10·90	0·025	SPL		
44	0·094	175·0	27·85	16·42	0·025	SPL		
45	0·090	144·3	22·97	11·90	0·017	SPL		
46	0·098	174·7	27·80	11·85	0·015	SPL		
47	0·091	—	—	—	—	—		
48	0·091	171·7	27·32	12·86	0·012	SPL		
Series 7, $f_{Rm} = 0{\cdot}047$, $f_{cm} = 63{\cdot}4$ MPa, $d = 12$ mm								
49	0·043	67·85	30·00	18·02	0·003	SPL	33·6	8·32
50	0·058	76·68	33·90	18·71	0·005	SPL		
51	0·042	65·14	28·80	16·71	0·012	SPL		
52	0·057	75·82	33·52	19·07	0·020	SPL		
53	0·040	79·18	35·01	18·16	0·009	SPL		
54	0·052	89·44	39·54	16·29	0·011	SPL		
55	0·043	82·35	36·41	21·48	0·004	SPL		
56	0·040	71·66	31·68	15·18	0·016	SPL		
Series 8, $f_{Rm} = 0{\cdot}061$, $f_{cm} = 63{\cdot}4$ MPa, $d = 16$ mm								
57	0·058	122·9	30·55	17·25	0·002	SPL	28·3	7·03
58	0·065	147·5	36·68	19·65	0·009	SPL		
59	0·056	124·6	30·99	20·18	0·009	SPL		
60	0·061	118·0	29·35	20·92	0·034	SPL		
61	0·059	80·26	19·96	19·91	0·035	SPL		
62	0·063	100·3	24·95	19·32	0·035	PO		
63	0·058	107·1	26·64	19·78	0·016	PO		
64	0·066	110·4	27·47	20·64	—	PO		

Table 6. Summary of test results of machined bars (continued on next page)

Specimen	f_R	P_{max}: kN	τ_{max}: MPa	$\tau_{0\cdot1}$: MPa	w_{15}: mm	Failure mode	$\tau_{max,av}$: MPa	$\tau_{max,av}/f_{bd}$ (MC2010)
Series 9, $f_{Rm} = 0{\cdot}066$, $f_{cm} = 63{\cdot}4$ MPa, $d = 20$ mm								
65	0·063	168·2	26·78	15·99	0·012	SPL	25·5	6·31
66	0·073	155·8	24·81	21·68	0·015	SPL		
67	0·068	198·9	31·66	17·96	0·019	SPL		
68	0·049	142·2	22·64	14·70	0·027	SPL		
69	0·066	185·2	29·47	17·34	0·017	PO		
70	0·069	157·4	25·06	14·80	0·019	PO		
71	0·063	127·3	20·26	15·21	0·022	PO		
72	0·069	145·4	23·14	16·36	0·026	PO		
Series 10, $f_{Rm} = 0{\cdot}081$, $f_{cm} = 74{\cdot}3$ MPa, $d = 12$ mm								
73	0·076	86·1	38·06	30·06	0·008	SPL	36·3	8·22
74	0·084	85·8	37·92	20·06	0·006	SPL		
75	0·083	84·1	37·19	23·00	0·015	SPL		
76	0·082	93·9	41·51	30·93	0·011	SPL		
77	0·077	60·1	26·57	—	—	SPL		
78	0·075	97·5	43·11	29·46	0·008	SPL		
79	0·096	64·3	28·42	23·11	0·006	SPL		
80	0·079	85·9	37·96	20·18	0·015	SPL		
Series 11, $f_{Rm} = 0{\cdot}095$, $f_{cm} = 74{\cdot}3$ MPa, $d = 16$ mm								
81	0·086	147·5	36·67	31·70	0·011	SPL	35·9	8·12
82	0·095	163·8	40·71	25·25	0·007	SPL		
83	0·097	117·4	29·20	28·87	0·010	SPL		
84	0·096	156·7	38·96	31·73	0·019	SPL		
85[a]	0·105	93·8	23·33	—	0·012	SPL		
86	0·094	116·7	29·02	29·02	0·014	SPL		
87	0·097	143·9	35·80	34·29	0·016	SPL		
88	0·093	164·9	41·00	32·67	0·013	SPL		
Series 12, $f_{Rm} = 0{\cdot}092$, $f_{cm} = 74{\cdot}3$ MPa, $d = 20$ mm								
89	0·089	204·5	32·55	23·69	0·016	SPL	33·8	7·64
90	0·100	213·7	34·01	24·59	0·027	SPL		
91	0·086	238·4	37·94	20·17	0·016	SPL		
92	0·094	243·5	38·76	30·24	0·015	SPL		
93	0·090	199·2	31·70	30·28	0·016	SPL		
94	0·098	222·4	35·40	35·09	0·008	SPL		
95[a]	0·091	131·0	20·84	—	0·019	SPL		
96	0·091	165·4	26·33	25·9	0·022	SPL		

[a] Disregarded result.
SPL, splitting failure; PO, pull-out failure.

Table 6. (continued)

Effect of bond index and bar diameter on bond strength

Test results concerning the bond strength τ_{max} are summarised in Figures 7–9; the results of each specimen with a machined rebar are plotted individually against the bond index f_R for both NSC (Figure 7(a)) and HSC specimens (Figure 7(b)). The mean bond strength of each series with hot-rolled commercial bars is also plotted in Figures 7–9. It is worth noting that the bond strength increases with the bond index and decreases with bar diameter. The increase in bond strength with bond index is more evident for the larger diameter rebars due to a stronger interaction between the ribs and the surrounding concrete; for smaller rebars, this interaction is limited by the porous concrete layer present in front of the ribs (Giuriani, 1982). The hot-rolled commercial bars showed a behaviour similar to the machined rebars. The larger bars, tested only in NSC specimens, exhibited a reduced bond strength with average values of 15·8–17·9 MPa for the 40 mm diameter bars and 16·3–18·3 MPa for the 50 mm diameter bars.

Specimen	f_R	P_{max}: kN	τ_{max}: MPa	$\tau_{0\cdot1}$: MPa	w_{15}: mm	Failure mode	$\tau_{max,av}$: MPa	$\tau_{max,av}/f_{bd}$ (MC2010)
Series 13, $f_{Rm} = 0{\cdot}095$, $f_{cm} = 41{\cdot}5$ MPa, $d = 12$ mm								
97	0·095	46·5	20·54	16·57	0·007	SPL	23·1	7·16
98	0·095	56·4	24·93	15·48	0·007	SPL		
99	0·095	59·4	26·26	14·11	0·011	SPL		
100	0·095	41·7	18·44	16·17	0·024	SPL		
101	0·095	62·4	27·58	18·17	0·009	PO		
102[a]	0·095	34·4	15·20	9·85	—	SPL		
103	0·095	54·5	24·10	17·08	0·013	SPL		
104	0·095	44·3	19·59	10·32	0·026	SPL		
Series 14, $f_{Rm} = 0{\cdot}089$, $f_{cm} = 41{\cdot}5$ MPa, $d = 20$ mm								
105	0·089	128·3	20·42	10·91	—	PO	20·8	6·45
106	0·089	150·7	23·98	10·85	0·027	SPL		
107	0·089	137·8	21·94	10·83	0·038	SPL		
108	0·089	122·1	19·43	8·56	0·038	PO		
109	0·089	123·9	19·71	12·40	0·030	SPL		
110	0·089	128·2	20·40	13·20	0·025	SPL		
111	0·089	123·1	19·59	9·44	0·021	SPL		
Series 15, $f_{Rm} = 0{\cdot}105$, $f_{cm} = 64{\cdot}8$ MPa, $d = 12$ mm								
112	0·105	76·9	33·99	33·27	0·018	SPL	32·5	8·04
113	0·105	57·5	25·40	27·58	0·007	PO		
114	0·105	80·0	35·35	31·09	0·017	Y		
115	0·105	79·3	35·07		0·003	Y		
116	0·105	75·8	33·53	31·90	0·010	SPL		
117	0·105	—	—	—	—	SPL		
118	0·105	77·3	34·15	—	0·005	SPL		
119	0·105	67·6	29·90	29·87	0·020	SPL		
Series 16, $f_{Rm} = 0{\cdot}079$, $f_{cm} = 64{\cdot}8$ MPa, $d = 20$ mm								
120	0·079	166·8	26·55	24·83		SPL	26·8	6·64
121	0·079	170·1	27·07	25·06	0·031	Y		
122	0·079	166·4	26·48	22·60	0·028	SPL		
123	0·079	163·1	25·95	21·41	0·037	SPL		
124	0·079	169·5	26·98	26·37	0·028	Y		
125	0·079	171·6	27·32	22·73	0·026	Y		
126	0·079	169·9	27·04	24·51	0·036	Y		
127	0·079	169·5	26·98	23·68	0·037	Y		
Series 17, $f_{Rm} = 0{\cdot}054$, $f_{cm} = 37{\cdot}6$ MPa, $d = 40$ mm								
128	0·054	391·8	15·59	4·68	—	SPL	15·8	6·11
129	0·054	299·8	11·93	3·63	—	SPL		
130	0·054	248·8	9·90	4·66	—	SPL		
131	0·054	547·4	21·78	4·01	—	SPL		
132	0·054	502·1	19·98	4·39	—	SPL		
Series 18, $f_{Rm} = 0{\cdot}072$, $f_{cm} = 37{\cdot}6$ MPa, $d = 40$ mm								
133	0·072	469·0	18·66	2·50	—	SPL	17·9	6·91
134	0·072	439·6	17·49	3·90	—	SPL		
135	0·072	431·0	17·15	3·85	—	PO		
136	0·072	403·9	16·07	4·56	—	PO		
137	0·072	500·4	19·91	7·27	—	SPL		
138	0·072	471·7	18·77	3·67	—	SPL		
139	0·072	431·3	17·16	4·53	—	SPL		

Table 7. Summary of test results of commercial bars (continued on next page)

Specimen	f_R	P_{max}: kN	τ_{max}: MPa	$\tau_{0\cdot1}$: MPa	w_{15}: mm	Failure mode	$\tau_{max,av}$: MPa	$\tau_{max,av}/f_{bd}$ (MC2010)
Series 19, $f_{Rm} = 0{\cdot}040$, $f_{cm} = 37{\cdot}6$ MPa, $d = 50$ mm								
140	0·040	688·8	13·93	2·00	—	SPL	16·3	6·74
141	0·040	663·3	14·49	5·22	—	SPL		
142	0·040	799·5	14·77	1·23	—	SPL		
143	0·040	777·9	18·81	4·32	—	SPL		
144	0·040	726·1	18·85	4·32	—	SPL		
145	0·040	547·0	17·04	3·01	—	SPL		
Series 20, $f_{Rm} = 0{\cdot}063$, $f_{cm} = 37{\cdot}6$ MPa, $d = 50$ mm								
146	0·063	612·2	16·66	3·23	—	SPL	18·3	7·55
147	0·063	468·5	17·54	2·32	—	SPL		
148	0·063	388·8	16·89	3·56	—	SPL		
149	0·063	855·3	20·36	6·36	—	SPL		
150	0·063	784·6	19·81	5·25	—	SPL		
151	0·063	654·2	18·49	3·75	—	SPL		

[a] Disregarded result.
SPL, splitting failure; PO, pull-out failure; Y, bar yielding.

Table 7. (continued)

Since the concrete strength $f_{cm,cube}$ varies between 35·5 and 74·3 MPa and it is widely recognised that bond strength is proportional to the tensile strength of concrete, the test results were normalised to the power of 2/3 of the compressive strength to allow for a better comparison between specimens made of different materials (Figure 8). By means of linear regressions of the experimental results, it can be seen that by increasing the relative rib area from 0·04 to 0·105, the bond strength of the 20 mm rebars increased by up to 40%. Conversely, within the same range of bond index, specimens with a 12 mm rebar showed a fairly constant bond strength.

The bond behaviour is strongly affected by bar diameter, as noted in previous studies on the size effect of highly confined ribbed bars with a short embedded length (Bamonte and Gambarova, 2007; Bazant and Sener, 1988); in fact, the bigger the bar diameter the lower the bond strength. Figure 9 shows the mean value of the normalised bond strength ($\tau_{max,av}/f_{cm,cube}^{2/3}$) of each series (both machined and commercial) in NSC plotted against bar diameter. It can be observed that the bond strength decreases by about 26% when the bar diameter increases from 12 to 50 mm and about by 13% for diameters from 20 to 50 mm (the cover/diameter ratio and the bond length/diameter ratio of all tested specimens being constant). One may also note the limited reduction in bond strength of the larger bars (40 and 50 mm) with a bond index lower than the minimum value required by Eurocode 2. These results are consistent with those of the pull-out tests presented by Ichinose *et al.* (2004), which showed a reduction in average bond strength from 12% to 54% with an increase in bar diameter from 17 to 50 mm; a larger difference was found in tests on bars with a higher relative rib area ($f_R > 0{\cdot}3$) and cover thickness equal to only 1·22 times the bar diameter due to splitting phenomena.

Comparison with the formulation proposed in MC2010

Since the tests were carried out with a short anchorage length (five times the bar diameter), the experimental bond–slip curve can be a useful tool to investigate the effectiveness of the local bond–slip law proposed by MC2010 (fib, 2013). For monotonic loading and for splitting failure in good bond conditions, the bond stress is calculated as a function of the slip δ according to

$$\tau = \tau_{bmax}(\delta/\delta_1)^{0\cdot4} \leqslant \tau_{u,split} \quad (4)$$

where $\delta_1 = 1$ mm, τ_{bmax} is the maximum bond stress for a pull-out failure, given by

$$\tau_{bmax} = 2{\cdot}5 f_{cm}^{0\cdot5} \quad (5)$$

$\tau_{u,split}$ is the bond strength for splitting failure, given by the following equation when transverse reinforcement is not present

$$\tau_{u,split} = 6{\cdot}5\left(\frac{f_{cm}}{25}\right)^{0\cdot25}\left(\frac{25}{d}\right)^{0\cdot20}\left[\left(\frac{c_{min}}{d}\right)^{0\cdot33}\left(\frac{c_{max}}{c_{min}}\right)^{0\cdot10}\right] \quad (6)$$

in which c_{max} and c_{min} are the maximum and minimum concrete cover (both equal to 4·5d in the present tests; Figure 2).

(a)

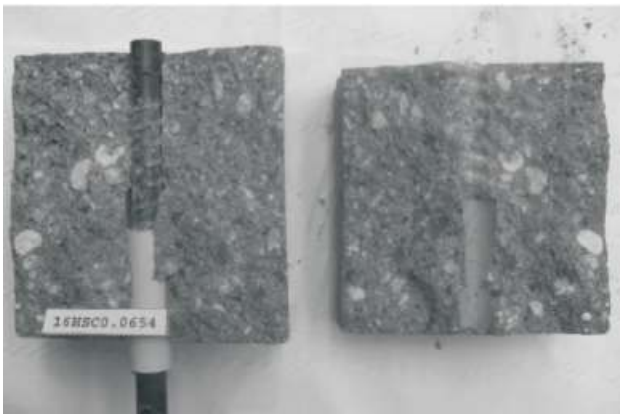

(b)

(c)

Figure 4. Typical splitting failure for normal-size bars in (a) NSC and (b) HSC. (c) Typical splitting failure for large-diameter bars

Figure 5 shows significant differences between the experimental bond–slip curves and the local bond–slip law proposed by MC2010, in terms of maximum bond strength, stiffness and slip at failure; these differences increase with the concrete strength and for small bar diameter. The MC2010 formulation markedly underestimates bond strength when smaller rebars (12 mm) with a higher bond index are used in HSC. Nevertheless, as shown in Tables 6 and 7, the mean bond strength of each series was always significantly greater than the design bond strength f_{bd} proposed by MC2010, as shown by

$$7. \quad f_{bd} = \alpha_2 f_{bd,0} < 2{\cdot}5 f_{bd,0} < 1{\cdot}5 \frac{f_{ck}^{0{\cdot}5}}{\gamma_{cb}}$$

where α_2 is a factor that takes into account the confining effects of concrete and $f_{bd,0}$ is the basic bond strength

$$8. \quad \alpha_2 = (c/d)^{0{\cdot}5} = 2{\cdot}12$$

$$9. \quad f_{bd,0} = \frac{\eta_1 \eta_2 \eta_3 \eta_4 (f_{ck}/25)^{0{\cdot}5}}{\gamma_{cb}}$$

in which the concrete cover in the pull-out specimen $c = 4{\cdot}5d$, $\eta_1 = 1{\cdot}75$ for ribbed bars, $\eta_2 = 1{\cdot}00$ since good bond conditions are assumed, $\eta_3 = (25/d)^{0{\cdot}3}$, $\eta_4 = 1{\cdot}00–0{\cdot}68$ depending on the steel grade f_{yk} ranging from 500 to 800 MPa and $\gamma_{cb} = 1{\cdot}5$ is the partial safety coefficient for bond.

As far as the machined bars are concerned, the experimental/design strength ratio ranges between 6·31 for the 20 mm diameter bar ($f_{Rm} = 0{\cdot}065$) in NSC and 8·39 for the 12 mm diameter bar ($f_{Rm} = 0{\cdot}081$) in NSC. The hot-rolled bars showed similar values, even for large bars with a bond index below the limit prescribed by Eurocode 2 ($f_R > 0{\cdot}056$ if $d > 12$ mm); in fact, the experimental/design strength ratio is 6·11 or 6·74 respectively for series 17 with 40 mm diameter bars ($f_{Rm} = 0{\cdot}054$) or series 19 with 50 mm diameter bars ($f_{Rm} = 0{\cdot}040$).

In Figure 9, the test results are also compared with the bond strength calculated according to MC2010 and with the size-effect analytical formulation proposed by Bamonte and Gambarova (2007). It is worth noting that MC2010 provides safety values of the bond strength for design purposes, as previously discussed, whereas the Bamonte and Gambarova (2007) formulation accurately fits all the test results since it was specifically calibrated for short embedded lengths with confined conditions. Furthermore, the semi-empirical equation proposed by MC2010 is based on a database that does not include tests with anchorage lengths shorter than ten diameters, corresponding to the minimum value required by Eurocode 2 (fib, 2014).

Effects on bond stiffness

Figures 10 and 11, concerning the bond stress $\tau_{0·1}$ measured at the unloaded-end slip value $\delta_u = 0{\cdot}1$ mm, provide useful information on the bond stiffness and, as a consequence, on the behaviour

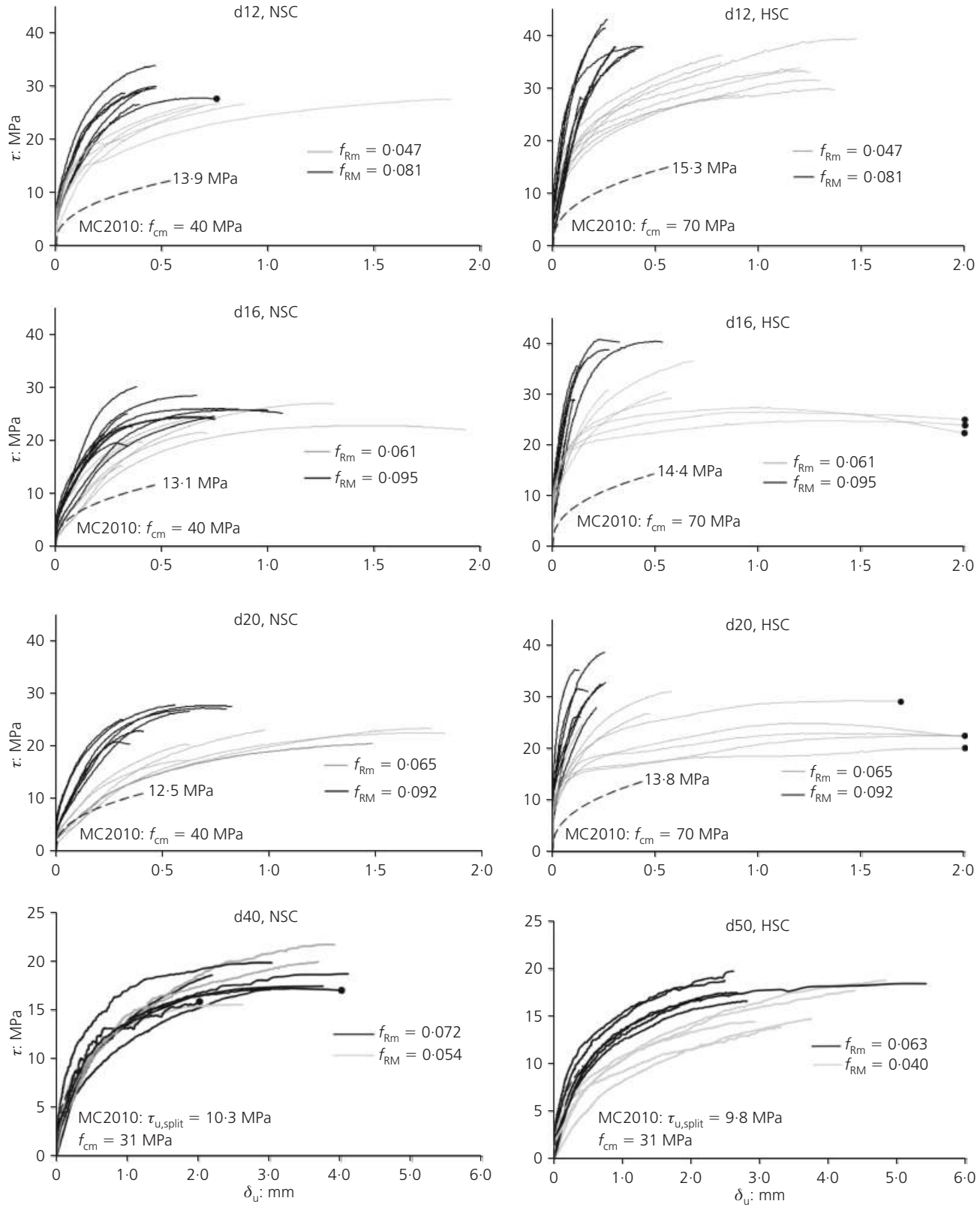

Figure 5. Bond stress (τ) plotted against unloaded-end slip (δ_u): comparison between test results of series with machined bars having different bond indexes but the same concrete strength (•, pull-out failure). Notation d12, d16, etc., refers to bar diameter, in mm

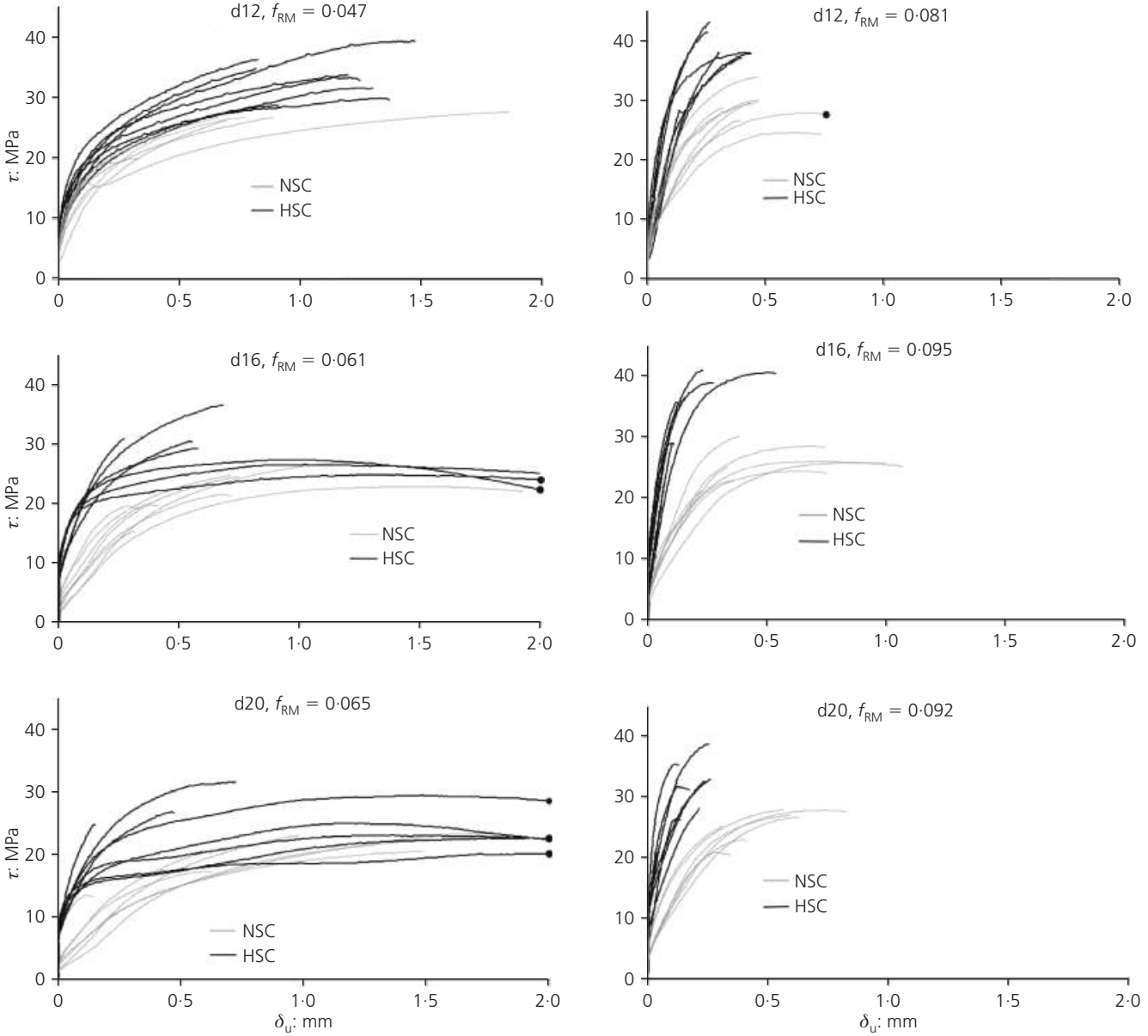

Figure 6. Bond stress (τ) plotted against unloaded-end slip (δ_u): comparison between test results of series with machined bars having the same bond index but different concrete strength (•, pull-out failure). Notation d12, d16, etc., refers to bar diameter, in mm

of the concrete member at service condition. Experimental results are plotted individually versus relative rib area (f_R), for both NSC and HSC specimens (Figure 10): the increase of the (secant) bond stiffness with both the relative rib area f_R (because of a more efficient interlocking between bar lugs and concrete) and the concrete strength (due to the lower porosity of HSC) can be noticed. For a given bond index, the bond stress $\tau_{0·1}$ is about twice as great in HSC specimens than in NSC specimens, and this difference tends to increase with the bond index. This is also evident in Figure 6 where the bond stress–slip curves are compared between series with a different concrete strength but the same bond index and bar diameter. Furthermore, within the tested range of bond index (0·04–0·072), the 40 and 50 mm diameter rebars showed a fairly low bond stiffness.

The influence of bar diameter on bond stiffness is better evidenced in Figure 11 where $\tau_{0·1}$ is plotted for each bar diameter (12–50 mm) in NSC; the experimental results show a clear size effect on bond stiffness, which is smaller in larger bars.

Effect on wedging action

In order to gain information on the bursting forces generated by the bar ribs, which tend to split the concrete cover around the bar, the transverse deformation of the cube specimens measured

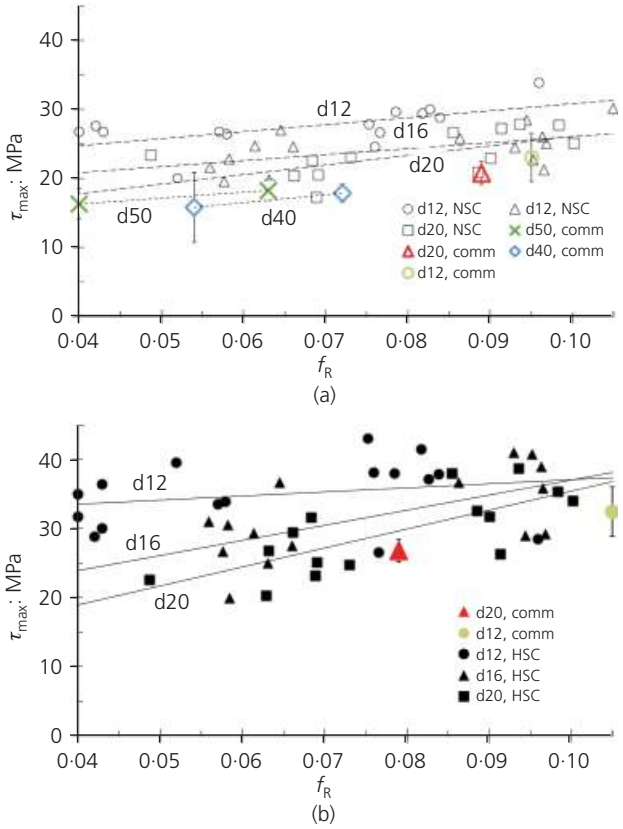

Figure 7. Bond strength (τ_{max}) plotted against relative rib area (f_R) for specimens in (a) NSC and (b) HSC. Notation d12, d16, etc. refers to bar diameter, in mm; comm represents commercial hot-rolled bar

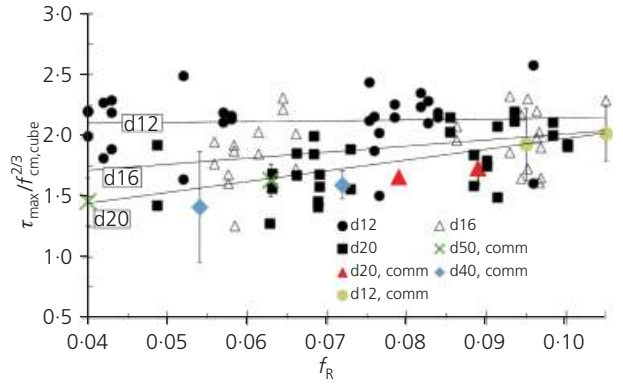

Figure 8. Normalised bond strength (τ'_{max}) plotted against relative rib area (f_R). Notation d12, d16, etc. refers to bar diameter, in mm; comm represents commercial hot-rolled bar

at an average bond stress of 15 MPa (w_{15}) is plotted against relative rib area f_R in Figure 12 for each specimen with machined rebars. The transverse deformation is calculated as the sum of the measurements given by the four LVDTs placed on each side of the specimen (Figure 2). Even though there is a wide scatter of

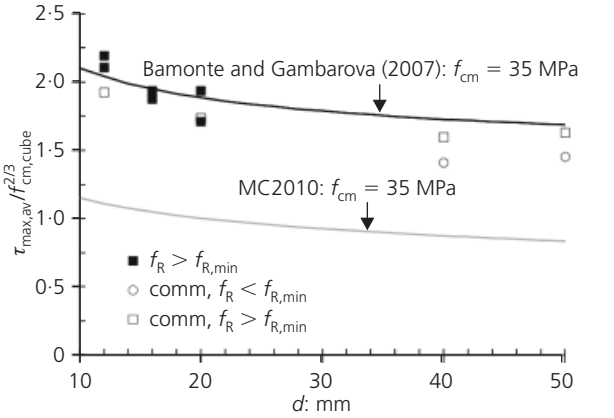

Figure 9. Normalised mean bond strength ($\tau'_{max,av}$) plotted against bar diameter (d) and comparison with local bond–slip laws

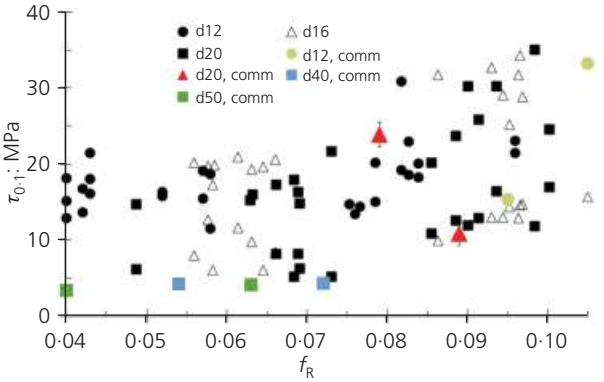

Figure 10. Influence of relative rib area on the bond stiffness: bond stress $\tau_{0\cdot1}$ measured at unloaded-end slip (δ_u) of 0·1 mm plotted against relative rib area (f_R). Notation d12, d16, etc. refers to bar diameter, in mm; comm represents commercial hot-rolled bar

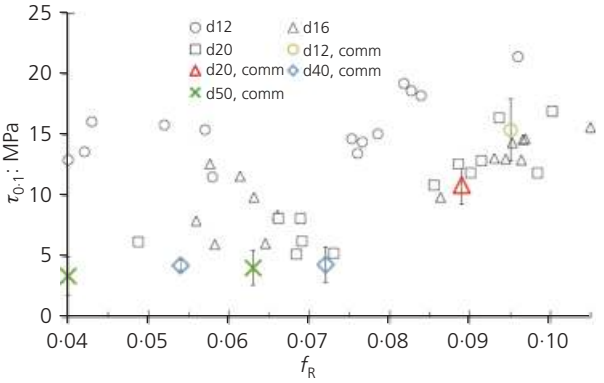

Figure 11. Influence of relative rib area on the bond stiffness in NSC: bond stress $\tau_{0\cdot1}$ measured at unloaded-end slip (δ_u) of 0·1 mm plotted against relative rib area (f_R). Notation d12, d16, etc. refers to bar diameter, in mm

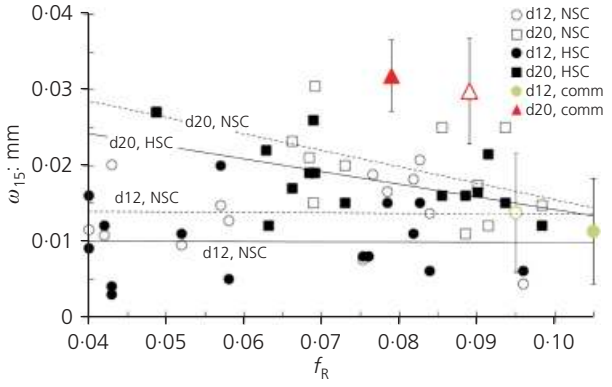

Figure 12. Transverse deformation (w_{15}) of the specimens plotted against bond index (f_R), at the bond stress of 15 MPa. Notation d12, d16, etc. refers to bar diameter, in mm; comm represents commercial hot-rolled bar

results, Figure 12 shows a clear and sizeable dependence of the splitting crack on the relative rib area, both in NSC and in HSC specimens. The transverse deformation w_{15} shows an upward trend with bar dimension and a downward trend with an increase in bond index.

The experimental results confirm the analytical studies of Cairns and Jones (1995b), who suggested a lower wedging action of an anchored bar with a higher relative rib area; this allows a higher bond strength to be achieved, as clearly shown in Figures 5, 7 and 8. Furthermore, it is worth pointing out the significant influence of bar dimension on bursting force (size effect), especially in rebars with a low bond index. By assuming that the measured transverse deformation is proportional to the radial force exerted by ribs, the test results indicate that the bursting action generated by 20 mm diameter bars is twice that generated by 12 mm diameter bars, both in NSC and in HSC for a bond index of 0·05; this difference reduces to 10% for a bond index of 0·10. Although it is difficult to accurately quantify the difference between the bursting force in HSC and NSC because of the wide scatter of the test results, the linear regressions in Figure 12 show the tendency of bond to exert a greater wedging action in NSC (dashed lines) rather than in HSC (continuous lines) for a given bar diameter. This is because of the lower porosity of HSC, which influences the local behaviour around the ribs of the rebars.

Concluding remarks

This paper has discussed an experimental programme of 151 pull-out tests carried out to better understand the influence of the relative rib area of reinforcing bars on bond. The experimental results provide information on bond strength, stiffness, size effect and wedge action generated by ribs.

The experiments were carried out on 12, 16 and 20 mm diameter machined bars of high steel grade, having a bond index ranging from 0·04 to 0·105, as well as on 12, 20, 40 and 50 mm diameter commercial hot-rolled bars with a bond index greater than 0·063. The 40 and 50 mm diameter bars were also tested with a bond index lower than the minimum value required by Eurocode 2. In the pull-out tests, all the rebars were embedded for a length of five times the bar diameter d in cubic specimens (without transverse reinforcement), with a cover of 4·5d.

The following conclusions can be drawn from the test results.

(*a*) Bond strength is strongly dependent on the relative rib area. For example, an increase in bond index from 0·04 to 0·10 leads to an increase of bond strength of up to 40%. This enhancement may be due to the lower wedging action generated by highly ribbed bars, which reduces the risk of splitting failure.
(*b*) The minimum bond strength, as determined from the specimens with a lower bond index, is significantly higher than the design value required by MC2010; this underlines the possibility of reducing the minimum value of relative rib area prescribed by codes without impairing the safety requirement of bond strength. This would enhance the structural ductility of RC members because of the greater strain penetration allowed by the increase in bond slip, especially if high-performance concrete is used.
(*c*) On the other hand, the tests results indicate that the adoption of a high bond index can limit the longitudinal splitting crack width, due to a reduced wedging action of the bar ribs.
(*d*) Finally, the test results confirm that bond behaviour is affected by a size effect, both in terms of strength and stiffness: for a bar diameter increasing from 12 to 50 mm, the reduction in bond strength is about 25% while the reduction in secant bond stiffness is greater than 70%.

Acknowledgements

The authors gratefully acknowledge the support of Leali S.p.A (Odolo, Italy) for financing a research project on large-diameter bars. Special acknowledgment goes to engineers A. Moreschi, M. Galuppi, M. Ferri and M. Cristini for their help in carrying out the tests. Finally, the authors thank technicians A. Delbarba and A. Coffetti, of the Laboratory P. Pisa of the University of Brescia, for their technical support.

Appendix

The geometric properties of the machined bars are shown in Table 8.

Bar No.	d_e: mm	a: mm	s: mm	f_R
Series 1 and 7, $f_{Rm} = 0{\cdot}047$				
1, 49	13·0	0·349	8·75	0·043
2, 50	13·0	0·469	8·75	0·058
3, 51	13·0	0·337	8·75	0·042
4, 52	13·0	0·466	8·75	0·057
5, 53	13·0	0·326	8·75	0·040
6, 54	13·0	0·418	8·75	0·052
7, 55	13·0	0·344	8·75	0·043
8, 56	13·0	0·321	8·75	0·040
Series 2 and 8, $f_{Rm} = 0{\cdot}061$				
9, 57	17·0	0·620	10·95	0·058
10, 58	17·1	0·686	10·95	0·065
11, 59	17·0	0·594	10·95	0·056
12, 60	17·0	0·656	10·95	0·061
13, 61	17·0	0·623	10·95	0·059
14, 62	17·1	0·671	10·95	0·063
15, 63	17·1	0·610	10·95	0·058
16, 64	17·1	0·703	10·95	0·066
Series 3 and 9, $f_{Rm} = 0{\cdot}065$				
17, 65	21·0	0·879	13·90	0·063
18, 66	21·0	1·023	13·90	0·073
19, 67	21·0	0·955	13·90	0·068
20, 68	21·0	0·671	13·90	0·049
21, 69	21·0	0·923	13·90	0·066
22, 70	21·0	0·966	13·90	0·069
23, 71	21·0	0·869	13·90	0·063
24, 72	21·0	0·963	13·90	0·069
Series 4 and 10, $f_{Rm} = 0{\cdot}081$				
25, 73	13·0	0·438	6·00	0·076
26, 74	13·0	0·470	6·00	0·084
27, 75	13·0	0·463	6·00	0·083
28, 76	13·0	0·458	6·00	0·082
29, 77	13·0	0·439	6·00	0·077
30, 78	13·0	0·431	6·00	0·075
31, 79	13·0	0·550	6·00	0·096
32, 80	13·0	0·450	6·00	0·079
Series 5 and 11, $f_{Rm} = 0{\cdot}095$				
33, 81	17·0	0·628	7·50	0·086
34, 82	17·1	0·694	7·50	0·095
35, 83	17·1	0·707	7·50	0·097
36, 84	17·2	0·698	7·50	0·096
37, 85	17·3	0·755	7·50	0·106
38, 86	17·0	0·685	7·50	0·094
39, 87	17·0	0·711	7·50	0·097
40, 88	17·1	0·679	7·50	0·093
Series 6 and 12, $f_{Rm} = 0{\cdot}092$				
41, 89	20·9	0·836	9·50	0·089
42, 90	21·0	0·949	9·50	0·100
43, 91	20·9	0·808	9·50	0·086
44, 92	21·1	0·880	9·50	0·094
45, 93	21·0	0·850	9·50	0·090
46, 94	21·1	0·927	9·50	0·098
47, 95	20·9	0·867	9·50	0·091
48, 96	21·0	0·862	9·50	0·091

Table 8. Geometric properties of machined bars

REFERENCES

Bamonte PF and Gambarova PG (2007) High-bond in NSC and HSC: a study on size effect and on the local bond stress–slip law. *Journal of Structural Engineering, ASCE* **133(2)**: 225–234.

Bazant ZP and Sener S (1988) Size effect in pull-out tests. *ACI Materials Journal* **85(5)**: 347–351.

Cairns J and Abdullah R (1995) An evaluation of bond pullout tests and their relevance to structural performance. *The Structural Engineer* **73(1)**: 179–185.

Cairns J and Jones K (1995a) The splitting forces generated by bond. *Magazine of Concrete Research* **47(171)**: 153–165.

Cairns J and Jones K (1995b) Influence of rib geometry on strength of lapped joints: an experimental and analytical study. *Magazine of Concrete Research* **47(172)**: 253–262.

Cairns J and Plizzari GA (2003) Towards a harmonised European bond test. *Material and Structures* **36(262)**: 498–506.

CEN (European Committee for Standardisation) (2004) Eurocode 2: EN 1992-1-1: Design of concrete structures. Part 1-1: General rules and rules for buildings. CEN, Brussels, Belgium.

Dancygier A and Katz A (2010) Bond between deformed reinforcement and normal and high-strength concrete with and without fibers. *Materials and Structures* **43(2)**: 839–856.

Darwin D and Graham EK (1993) Effect of deformation height and spacing on bond strength of reinforcing bars. *ACI Structural Journal* **90(6)**: 646–657.

Darwin D, McCabe SL, Idun EK and Schoenekase SP (1992) Development length criteria: bars not confined by transverse reinforcement. *ACI Structural Journal* **89(6)**: 709–720.

Eligehausen R and Mayer U (2000) *Investigation on the Influence of the Relative Rib Area of Reinforcement on the Structural Behaviour of Reinforced Members in the Serviceability and Ultimate Limit State*. Deutscher Ausschuss für Stahlbeton, Beuth, Berlin, Germany (in German).

Eligehausen R, Popov EP and Bertero VV (1983) *Local Bond Stress–slip Relationships of Deformed Bars Under Generalized Excitations*. University of California, Berkeley, CA, USA, Report UCB/EERC 83-23.

fib (International Federation for Structural Concrete) (2013) *Model Code for Concrete Structures 2010*. Ernst & Sohn, Berlin, Germany.

fib (2014) *Task Group 4.5: Bond Models, Convenor J. Cairns. Bond and Anchorage of Reinforcement – Background to Revisions in the fib Model Code 2010* – final draft, in press. fib, Lausanne, Switzerland.

Gambarova PG and Rosati GP (1997) Bond and splitting in bar pull-out: behavioural laws and concrete-cover role. *Magazine of Concrete Research* **48(6)**: 99–110.

Gambarova PG, Plizzari GA, Balazs GL *et al.* (2000) Bond mechanics including pull-out and splitting failures. In *fib Bulletin 10: Bond of Reinforcement in Concrete*. fib, Lausanne, Switzerland, pp. 1–98.

Giuriani E (1982) On the effective axial stiffness of a bar in cracked concrete. In *Bond in Concrete* (Bartos P (ed.)). Applied Science, London, UK, pp. 107–126.

Giuriani E and Plizzari GA (1998) Interrelation of splitting and flexural cracks in R. C. beams. *Journal of Structural Engineering, ASCE* **124(9)**: 1032–1040.

Giuriani E, Plizzari GA and Schumm C (1991) Role of stirrups and residual tensile strength of cracker concrete on bond. *Journal of Structural Engineering, ASCE* **117(1)**: 1–18.

Harajli MH, Hout M and Jalkh W (1995) Local bond stress–slip behaviour of reinforcing bars embedded in plain and fiber concrete. *ACI Materials Journal* **92(4)**: 343–354.

Ichinose T, Kanayama Y, Inoue Y and Bolander JE (2004) Size effect on bond strength of deformed bars. *Construction and Building Materials* **18(7)**: 549–558.

ISO (International Organization for Standardization) (2010) EN 15630-1: Steel for the reinforcement and prestressing of concrete – Test methods – Part 1: Reinforcing bars, rod and wire. ISO, Geneva, Switzerland.

Jansson A, Lofgren I, Lundgren K and Gylltoft K (2012) Bond of reinforcement in self-compacting steel-fibre-reinforced concrete. *Magazine of Concrete Research* **64(7)**: 617–630.

Metelli G, Cominoli L, Panteghini A and Plizzari GA (2010) *Numerical and Experimental Study on the Use of Large Diameter Ribbed Bars in Concrete Structures*. DICATA, University of Brescia, Brescia, Italy, Technical report 11 (in Italian).

Plizzari GA, Deldossi MA and Massimo S (1998) Transverse reinforcement effects on anchored deformed bars. *Magazine of Concrete Research* **50(2)**: 161–177.

Reinhardt HW and van der Veen C (1990) Applications of fracture mechanics to reinforced concrete. In *Splitting Failure of a Strain-softening Material Due to Bond Stresses* (Carpinteri A (ed.)). Elsevier, Barking, UK, pp. 333–346.

Rhem G (1969) *Evaluation Criteria for High-bond Rebars*. Festschrift Rüsch. Ernst and Sohn, Berlin, (in German).

Rilem/CEB/FIP (1978) *Bond Test for Reinforcing Steel 2: Pull-out Test. Recommendation RC6*. Rilem, Bagneux, France.

Tepfers R (1973) *A Theory of Bond Applied to Overlapped Tensile Reinforcement Splices for Deformed Bars*. Chalmers University of Technology, Goteborg, Sweden, Publication 73/2.

Walker PR, Batayneh MK and Regan PE (1999) Measured and design bond strengths of deformed bars, including the effect of lateral compression. *Magazine of Concrete Research* **51(1)**: 13–26.

Wildermuth A and Hofmann J (2012) Effect of the bond behaviour of rebars and its evaluation by simplified test specimens. *Proceedings of the 4th International Conference on Bond in Concrete, Brescia, Italy*, **1**, 75–80.

Xu F, Wu ZM, Zheng JJ, Hu Y and Li QB (2011) Experimental study on the bond behavior of reinforcing bars embedded in concrete subjected to lateral pressure. *Journal of Materials in Civil Engineering* **24(1)**: 125–133.

Zuo J and Darwin D (2000) Bond slip of high relative rib area under cycling loading. *ACI Structural Journal* **97(2)**: 331–335.